

pubs.acs.org/JACS Article

# Waste-Free Fully Electrically Fueled Dissipative Self-Assembly System

Dipankar Barpuzary, Paul J. Hurst, Joseph P. Patterson, and Zhibin Guan\*



Cite This: J. Am. Chem. Soc. 2023, 145, 3727-3735



**Read Online** 

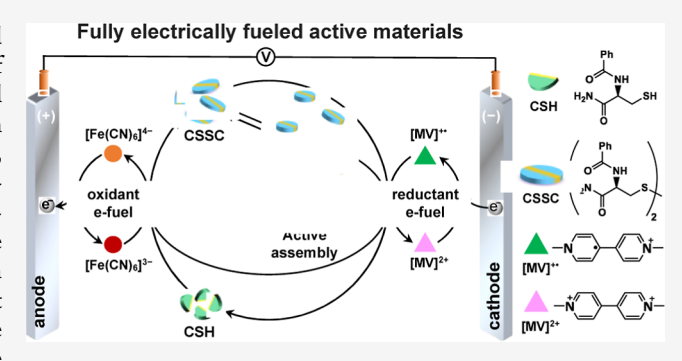
**ACCESS** 

III Metrics & More

Article Recommendations

Supporting Information

**ABSTRACT:** The importance and prevalence of energy-fueled active materials in living systems have inspired the design of synthetic active materials using various fuels. However, several major limitations of current designs remain to be addressed, such as the accumulation of chemical wastes during the process, unsustainable active behavior, and the lack of precise spatiotemporal control. Here, we demonstrate a fully electrically fueled (efueled) active self-assembly material that can overcome the aforementioned limitations. Using an electrochemical setup with dual electrocatalysts, the anodic oxidation of one electrocatalyst (ferrocyanide,  $[Fe(CN)_6]^{4-}$ ) creates a positive fuel to activate the self-assembly, while simultaneously, the cathodic reduction of the



other electrocatalyst (methyl viologen,  $[MV]^{2+}$ ) generates a negative fuel triggering fiber disassembly. Due to the fully catalytic nature for the reaction networks, this fully e-fueled active material system does not generate any chemical waste, can sustain active behavior for an extended period when the electrical potential is maintained, and provides spatiotemporal control.

#### ■ INTRODUCTION

Dissipative self-assemblies (DSAs) are prevalent in nature and have evolved myriad dynamic structures and activities to regulate critical cellular functions such as cell division, proliferation, self-healing, and homeostasis. 1,2 Existing far away from thermodynamic equilibrium, such active assemblies in living systems persist in highly organized low-entropy states sustained by constant energy intake from chemical fuels.<sup>3</sup> For example, dynamic actin filaments and microtubules are formed by supramolecular polymerizations when the precursor proteins are activated by chemical fuels like adenosine 5triphosphate (ATP) or guanosine triphosphate (GTP).4 Such active assemblies maintain dynamic instability in living systems with constant fuel intake and dissipation. Notably, regulated by the intricate and locally modulated intracellular signaling networks, cells can achieve precise spatiotemporal control over natural DSAs, which is critical for their biological functions.

Inspired by such biological active systems, several synthetic DSA systems have been created by mainly using chemicals<sup>5–9</sup> or light<sup>10–12</sup> as the fuel sources. DSAs of various building blocks, such as organic molecules,<sup>5,13–16</sup> peptides,<sup>14,17,18</sup> DNAs,<sup>19,20</sup> and nanoparticles,<sup>21</sup> were generated by using chemical fuels including alkylating agents,<sup>5</sup> carbodiimides,<sup>14,15</sup> ATP/GTP,<sup>19,22–25</sup> and oxidants.<sup>13,26,27</sup> Alternatively, DSAs of small molecules,<sup>28,29</sup> proteins,<sup>11</sup> and particles<sup>10,30</sup> were formed using light as the fuel. Despite great progress being made, several major challenges remain to be addressed in the field. For chemical-fueled DSA system, one major challenge is waste accumulation that causes closed DSA systems to change with

time, not only limiting the lifetime of the active states but also prohibiting sustainable operation.<sup>31</sup> While light is a cleaner fuel compared to chemical fuels, it is limited by penetration depth and has a lower efficiency in generating the activated state.<sup>12</sup> Moreover, light-driven DSAs are limited to special substrates having light-sensitive motifs (e.g., photoswitches like azobenzenes or spiropiranes),<sup>32,33</sup> limiting their general applicability.

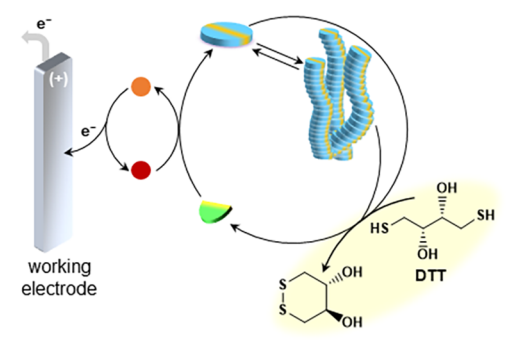
To address the aforementioned challenges, our lab has been developing electrically fueled DSA systems.<sup>34</sup> Electricity is a clean energy and readily accessible and can be administered with precise spatiotemporal control. Electric potential has also been used to control supramolecular interactions including out-of-equilibrium assemblies.<sup>35–37</sup> In our previous study, we described a hybrid DSA system that is composed of an electrochemical oxidation for activating the self-assembly and a chemical reduction for deactivating the system for disassembly.<sup>34</sup> While this system demonstrates spatiotemporal control over the self-assemblies, the dissipative reduction cycle still generates a chemical waste (Figure 1a). In a closed system, the reductant (dithiothreitol, DTT) is gradually consumed, while the oxidized DTT waste accumulates with time. As a result, the

Received: December 12, 2022 Published: February 6, 2023



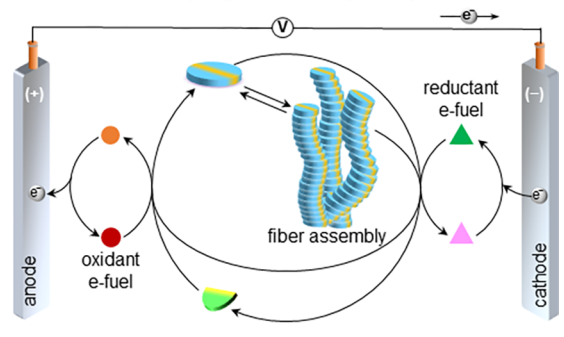


#### a. Previous work (hybrid system, JACS 2022):

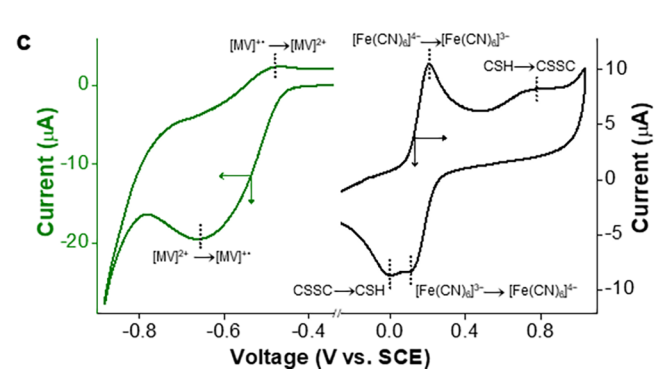


- · Hybrid fueling system
- · Chemical reduction creates waste
- · Cannot sustain for a long time

#### b. Current work (fully e-fueled system):



- Fully e-fueled system
- No waste generation
- Can sustain for a long time



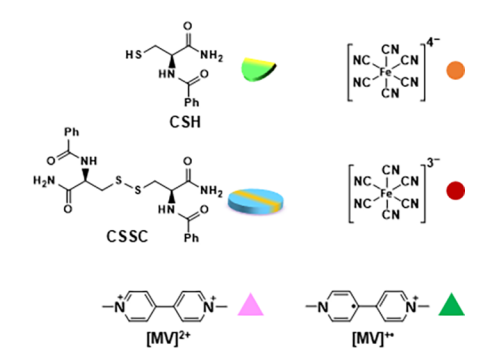


Figure 1. Design of fully e-fueled active self-assembly system. (a) Our previously reported hybrid design combining an e-fuel for CSH oxidation and DTT as a chemical reductant for CSSC reduction showing generation of chemical waste. (b) Illustration of the current new design of fully e-fueled DSA of CSH/CSSC system mediated by dual electrocatalytic cycles. Under applied electrical potential, at the anode,  $[Fe(CN)_6]^{4-}$  is electrochemically oxidized to  $[Fe(CN)_6]^{3-}$  that further oxidizes CSH into CSSC for fiber assembly. Simultaneously, at the cathode,  $[MV]^{2+}$  is electrochemically reduced to produce  $[MV]^{+\bullet}$ , which further reduces CSSC to CSH and induces disassembly. (c) CV plot showing electrocatalytic oxidation and reduction of CSH and CSSC in the presence of  $[Fe(CN)_6]^{4-}$  and  $[MV]^{2+}$  through in situ generation of  $[Fe(CN)_6]^{3-}$  and  $[MV]^{+\bullet}$  at anodic and cathodic half cycles, respectively.

system constantly evolves with time and the DSA process cannot be sustained over an extended period even with an electrical potential applied.

To overcome the limitations as discussed above, here, we report a fully electrically fueled (e-fueled) DSA system that does not generate any chemical waste and can be sustained for an extended period of time by electrical energy. To achieve this, we integrate two electrocatalytic cycles—one creating a catalytic oxidant and the other generating a catalytic reductant both electrochemically—at two separate electrodes to drive the assembly and disassembly simultaneously (Figure 1b). Specifically, electrochemical oxidation of one catalyst at the anode generates a catalytic oxidant (positive fuel) that oxidizes a cysteine derivative (CSH) into its corresponding cystine derivative (CSSC), initiating self-assembly into microfibers (Figure 1b).<sup>38</sup> Simultaneously, electrochemical reduction of another catalyst at the cathode produces a catalytic reductant (negative fuel) that reduces CSSC back to CSH and triggers disassembly. By integrating the anodic and cathodic half cycles into one system, we have established a fully electrically fueled active self-assembly system that is completely waste-free, with spatiotemporal control, and can be sustained over an extended period.

#### RESULTS AND DISCUSSION

Design of Fully e-Fueled DSA System. To achieve a fully e-fueled DSA system, first, we need to identify two electrocatalytic cycles that meet the following criteria: (1) the two homogeneous electrocatalysts (or redox mediators) have good redox stability and reversibility during the e-fueled selfassembly cycles; (2) the two electrocatalytic cycles are compatible with each other and with the DSA system (i.e., the two catalysts do not have undesired reactions with each other or with the DSA system); (3) the redox potentials of the two redox mediators match the redox potential of the selfassembly building block used for DSA. With these considerations in mind, we chose ferrocyanide ( $[Fe(CN)_6]^{4-}$ ) as the mediator for electrochemical oxidation at the anode and methyl viologen (1,1'-dimethyl-4,4'-bipyridinium dichloride, [MV]<sup>2+</sup>) as the mediator for electrochemical reduction at the cathode. For simplicity, we employed the same cysteine derivative (CSH) used in our prior studies as the monomer in this study.  $^{\hat{1}3,34}$  Our previous work  $^{34}$  showed  $[Fe(CN)_6]^{4-}$  as an effective redox mediator for electrochemical oxidation of CSH to its cystine derivative CSSC, which was adopted in the current study for the electrochemical oxidation half cycle. For the reduction half cycle, we chose  $[MV]^{2+}$  as the electrocatalyst because its redox potential is suitable for CSSC reduction and previous reports have shown reduced methyl viologen ([MV]+•) to effectively reduce disulfides into thiols.<sup>3</sup>

Furthermore, [MV]<sup>2+</sup> is a common, robust electrocatalyst used for various reduction-based applications including electro-chromic devices, 42 enzymatic assays, 43,44 organic redox flow batteries,  $^{45}$  and switchable redox indicators.  $^{45}$  Notably, the compatibility of  $[Fe(CN)_6]^{4-}/[Fe(CN)_6]^{3-}$  with  $[MV]^{2+}/[Fe(CN)_6]^{3-}$ [MV]+• redox pairs has been demonstrated previously, 46,47 and various Fe<sup>II</sup>/Fe<sup>III</sup> cycles with viologen derivatives as redox mediators were utilized in electrochromic cells to achieve reversible color switching. 48,49 In our design, we combine  $[Fe(CN)_6]^{4-}$  and  $[MV]^{2+}$  as two redox mediators and simultaneously activate them at two electrodes by electric potential to catalytically generate  $[Fe(CN)_6]^{3-}$  as the oxidant at the anode (positive fuel) and [MV]+• as the reductant at the cathode (negative fuel). By coupling the catalytic electrochemical redox reaction networks to the dynamic interconversion between CSH and CSSC, we created a fully e-fueled active supramolecular assembly system (Figure 1b) in which the anodic oxidation cycle promotes CSSC production and selfassembly into fibers while the cathodic reduction cycle simultaneously reduces CSSC back to CSH to trigger disassembly. With complete electrocatalytic cycles for both the assembly and disassembly processes, the active system does not create any chemical waste and can be sustained by electrical potential for an extended period, while maintaining precise spatiotemporal control similar to our previous hybrid system.<sup>34</sup> To confirm the viability of our design, we performed cyclic voltammetry (CV) experiments to monitor the oxidation and reduction of CSH and CSSC in the presence of [Fe(CN)<sub>6</sub>]<sup>4-</sup> and [MV]<sup>2+</sup> in deoxygenated phosphate buffer at pH 7. CV plot in Figure 1c displayed a low magnitude for cathodic current (higher for anodic), indicating involvement of  $[Fe(CN)_6]^{4-}$  in CSH oxidation. Conversely,  $[MV]^{2+}$  showed significantly enhanced cathodic current, suggesting its participation in the reduction of both CSSC and  $[Fe(CN)_6]^{3-}$ . Figure 1c also depicts a reversible single electron transfer peak for [MV]<sup>2+</sup> to [MV]<sup>+•</sup> reduction at -0.66 V versus saturated calomel electrode (SCE), while that for  $[Fe(CN)_6]^{4-}$  oxidation appeared at 0.21 V versus SCE. Overall electrochemistry involving the oxidation and reduction of dual electrocatalysts can be shown as follows

$$[Fe(CN)_6]^{4-} - e^- \rightarrow [Fe(CN)_6]^{3-}, \qquad E^\circ = 0.21 \text{ V}$$
(1)

$$[MV]^{2+} + e^{-} \rightarrow [MV]^{+\bullet}, \qquad E^{\circ} = -0.66 \text{ V}$$
 (2)

$$[MV]^{2+} + [Fe(CN)_6]^{4-} \rightarrow [MV]^{+\bullet} + [Fe(CN)_6]^{3-},$$
  
 $E^{\circ} = -0.87 \text{ V}$  (3)

From the CV plot, the difference between the midpoint potentials of  $[MV]^{2+}$  and  $[Fe(CN)_6]^{4-}$  is -0.87 V, suggesting that direct reaction between  $[Fe(CN)_6]^{4-}$  and  $[MV]^{2+}$  (eq 3) is thermodynamically unfavorable ( $\Delta G_{\text{rxn}} = -nFE_{\text{rxn}}^{\circ} > 0$ ). In contrast, when their respectively reduced and oxidized species (i.e., [MV]<sup>+•</sup> and [Fe(CN)<sub>6</sub>]<sup>3-</sup>) come in contact, electron transfer from [MV]<sup>+•</sup> to [Fe(CN)<sub>6</sub>]<sup>3-</sup> (reverse reaction of eq 3) is spontaneous. Similarly, the reduction of CSSC appears at ~0 V versus SCE (Figure 1c), which was not observed in earlier work<sup>34</sup> of [MV]<sup>2+</sup>-free hybrid system, indicating that electron transfer from [MV]+• to CSSC mediated its reduction to regenerate CSH (Figure 1a). The CV analysis validates the use of  $[Fe(CN)_6]^{4-}$  and  $[MV]^{2+}$  as dual electrocatalysts to mediate reversible conversion between CSH and CSSC without forming any chemical waste.

**Model Kinetic Study.** To further test the feasibility of fully e-fueled DSA design, we conducted a model study using ultraperformance liquid chromatography (UPLC) and UV-vis spectroscopy analyses to respectively monitor the formation and decay of the disulfide species and [MV]+• in situ during repetitive electrochemical cycles. For this purpose, customized electrochemical cells were built by parallelly placing two indium tin oxide (ITO)-coated glass slides inside a 3D-printed square plastic mold (for UPLC, Figure S2) and a plastic cuvette (for UV-vis, Figure S3) such that the working electrodes reside on one side while the counter and reference electrodes (both fabricated onto one ITO slide by chemical etching) reside on its opposite (Figures 2a and S1). The

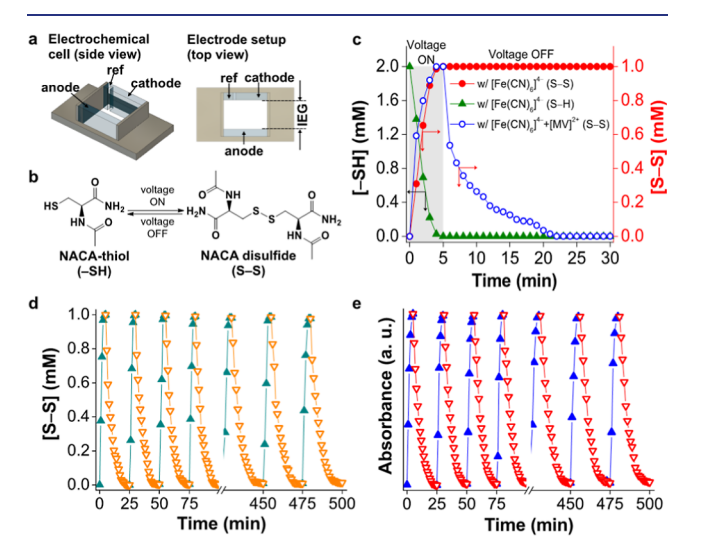


Figure 2. Model kinetic study. (a) Customized electrochemical cell with one ITO slide as counter and reference electrodes and one as the working electrode parallelly placed at an interelectrode gap (IEG) of 500  $\mu$ m. (b) Reaction scheme depicting e-fueled oxidation of NACA thiol to NACA disulfide by electrochemical oxidation mediated by [Fe(CN)<sub>6</sub>]<sup>4-</sup> and reversal by electrochemical reduction mediated by [MV]<sup>2+</sup>. (c) UPLC analysis showing in situ formation of NACA disulfide [S-S] and decay into thiol [-SH] during electrochemical redox cycle [initial solution: pH 7, 2 mM NACA-thiol, 120 mM  $[Fe(CN)_6]^{4-}$ , with (open circle) and without (filled symbols) 160 mM  $[MV]^{2+}$ ]. A bias of 0.8 V (vs ITO reference) was applied for 5 min and then stopped for next 20 min. (d,e) Reversible formation and decay of NACA disulfide ([S-S]) and [MV]+• with 0.8 V (vs ITO reference) voltage on for ~5 min (filled tringles), followed by gradual decay in ~20 min under voltage off condition (empty triangles) for 20 consecutive cycles.

electrochemical cells were purged by argon prior to sealing to ensure an oxygen-free environment during the entire analysis. To avoid complication caused by CSSC gelation, a close analogue of CSH, N-acetylcysteine amide (NACA, Figure 2b), was used as a model compound in the UPLC and UV-vis experiments. UPLC analysis (Figure 2c) of electrochemical oxidation of NACA in the presence of  $[Fe(CN)_6]^{4-}$  but without [MV]2+ showed that the disulfide derivative (red filled circles) was quickly formed after applying 0.8 V voltage (vs ITO reference) with simultaneous decay of NACA monomer (green filled triangles), which remained as such after the electrical potential was removed. Repeating the same experiment with inclusion of [MV]2+ in the solution led to a very different behavior. After a nearly identical initial profile for disulfide formation, it decayed gradually within ~15 min after

voltage removal (Figure 2c, blue empty circles) due to reduction by [MV]+• electrochemically generated at the cathode. Notably, the cycle could be repeated many times without noticeable change of the kinetic profile (tested up to 20 runs, Figure 2d), supporting good reversibility of our fully e-fueled design. To follow the reduction process, we quantified in situ formation and decay of [MV]+• during electrochemical cycles of the same solution described above by monitoring its characteristic UV-vis absorption at 607 nm (molar extinction coefficient,  $\varepsilon = 13,900 \text{ M}^{-1}\text{ cm}^{-1}$ ) (Figure 2e).<sup>49</sup> UV-vis data proved rapid generation of [MV]+• after applying a 0.8 V electrical potential (vs ITO reference), followed by gradual decay in ~15 min after the voltage was removed, during which [MV]\*\* was consumed through reduction of NACA disulfide in the solution. Again, the process can be repeated many cycles without noticeable change of the kinetic profile, further supporting the stability and reversibility of the system. These results have clearly established that the dual electrocatalytic cycles are stable and reversible and work cooperatively to the formation and dissipation of the disulfide derivative.

Transient Self-Assembly of Fibers. The model kinetic study revealed the transient formation of disulfide species having a certain lifetime that is governed by electrochemical production of the catalytic species and their diffusion from electrodes toward bulk solution. In contrast to normal chemical-fueled DSAs in which chemical fuels are irreversibly consumed to generate waste with time, in our fully e-fueled system, the fuels (i.e.,  $[Fe(CN)_6]^{3-}$  and  $[MV]^{+\bullet}$ ) are electrocatalytically produced in situ to sustain the out-ofequilibrium self-assembly without any waste generation. To achieve transient DSA, we first optimized the concentrations of initial species (CSH, [Fe(CN)<sub>6</sub>]<sup>4-</sup>, [MV]<sup>2+</sup>), the operating voltage, and the interelectrode gaps. On the basis of the optimization, the transient DSA was conducted in pH 7 phosphate buffer with 2 mM CSH, 120 mM  $[Fe(CN)_6]^{4-}$ , 160 mM  $[MV]^{2+}$ , and 25  $\mu$ M Nile red (as an intercalation dye used for confocal laser scanning microscopy, CLSM)<sup>13</sup> in a sealed electrochemical cell (Figure 2a) under an oxygen-free environment. As revealed by CLSM, fibers grew from the surface of the working electrode shortly after a 0.8 V (vs ITO reference) electrical potential was applied between the working and counter electrodes (Figure 3a, Movie S1). When the current was turned off at 10 s, the fibers began to disassemble and eventually disappeared after 10 min. Cryo-transmission electron microscopy (cryo-TEM) showed an average diameter of ~18 nm for CSSC fibers collected during e-fueled selfassembly (Figure 3b). These fibers also stack and entangle and appeared as larger assemblies over time (Figure S4). Consistent with our early kinetic study (Figure 2d,e) and previous report,<sup>34</sup> when an electrical potential is applied to the system, the oxidative electrocatalytic cycle creates [Fe-(CN)<sub>6</sub>]<sup>3-</sup>, which oxidizes CSH to CSSC and initiates fiber assembly from the anode surface. Simultaneously, the reductive electrocatalytic cycle generates  $[MV]^{+\bullet}$  at the cathode. Upon depletion of  $[Fe(CN)_6]^{3-}$  when the voltage is turned off, the in situ generated  $[MV]^{+\bullet}$  will diffuse from the cathode toward bulk solution, initially reducing CSSC at the fiber front and then in the body of the gel. Enabled by the dual electrocatalytic cycles, the transient assembly is completely waste-free and reversible.

In agreement with the reversibility observed in the model kinetic study (Figure 2d,e), the transient self-assembled fibers could be grown and dissipated repetitively by turning the

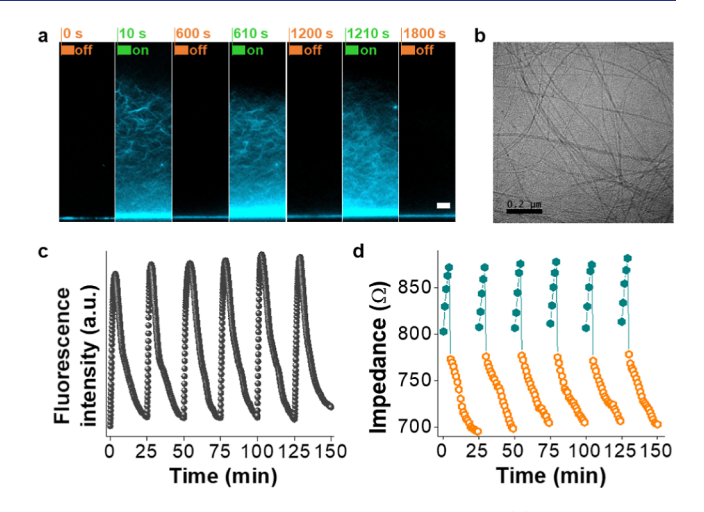


Figure 3. Fully e-fueled transient self-assembly. (a) Fully e-fueled transient self-assembly of CSSC fibers (pH 7, 2 mM CSH, 120 mM  $[Fe(CN)_6]^{4-}$  and 160 mM  $[MV]^{2+}$ ). Fibers grow perpendicularly from the anode (located at the bottom) surface on applying 0.8 V (vs ITO reference) potential for ~10 s, followed by disassembly when the voltage was turned off for ~10 min. The time points of each snapshot extracted from CLSM video file are provided on the top. The scale bar is 10  $\mu$ m. (b) Cryo-TEM image of CSSC fibers formed during fully efueled assembly after applying 0.8 V (vs ITO reference) potential for 30 s. The scale bar is 200 nm. (c) Reversible changes in average fluorescence intensity vs time obtained from CLSM to show repetitive growth and decay of fibers when the voltage was turned on and off, repetitively. (d) Reversible changes of single-frequency (10 kHz) electrochemical impedance when the voltage was turned on and off repetitively.

voltage on and off. The repetitive growth and shrinkage of fibers with time were quantified by the fluorescence intensity plot, which correlates to the quantity of the self-assembled fibers (Figure 3c). This shows very similar growth and shrinkage profiles for multiple repeating cycles, confirming the stability and reversibility of the fully e-fueled DSA. The timescales for CSSC fiber growth cycles (Figure 3c) are comparable to those for the oxidation of NACA (Figure 2c,d), but those for fluorescence decay cycles due to CSSC fiber dissolution (~18 min, voltage off, Figure 3c) are slightly longer than the reduction of NACA dimer in homogeneous solution (~14 min, voltage off, Figure 2c,d). This is attributed to slower diffusion of [MV]+• to CSSC gel and hence slower reduction of CSSC in the gel state than NACA dimer in the homogeneous solution. To further demonstrate that the system could dynamically transduce electronic inputs related to sensing, actuation, and computation, single-frequency (10 kHz) electrochemical impedance spectroscopy (EIS) was concurrently used to probe the impedance changes of the fully e-fueled DSA on the same three-electrode cell as used for CLSM (Figure 3d). The impedance of the system increased sharply upon application of 0.8 V (vs ITO reference) for 10 s due to the growth of fiber networks between electrodes and dropped after the potential was returned to 0 V. Presumably, the increase in impedance is caused by the inhibition of ionic currents between electrodes due to impeded charge transport through the self-assembled fiber network. When the voltage is removed, the impedance returns to the initial value, indicating complete dissolution of the fibers formed in the system. The impedance change profile parallels the fluorescence intensity for multiple cycles of turning the voltage on and off. The reproducible patterns observed for the fluorescence intensity

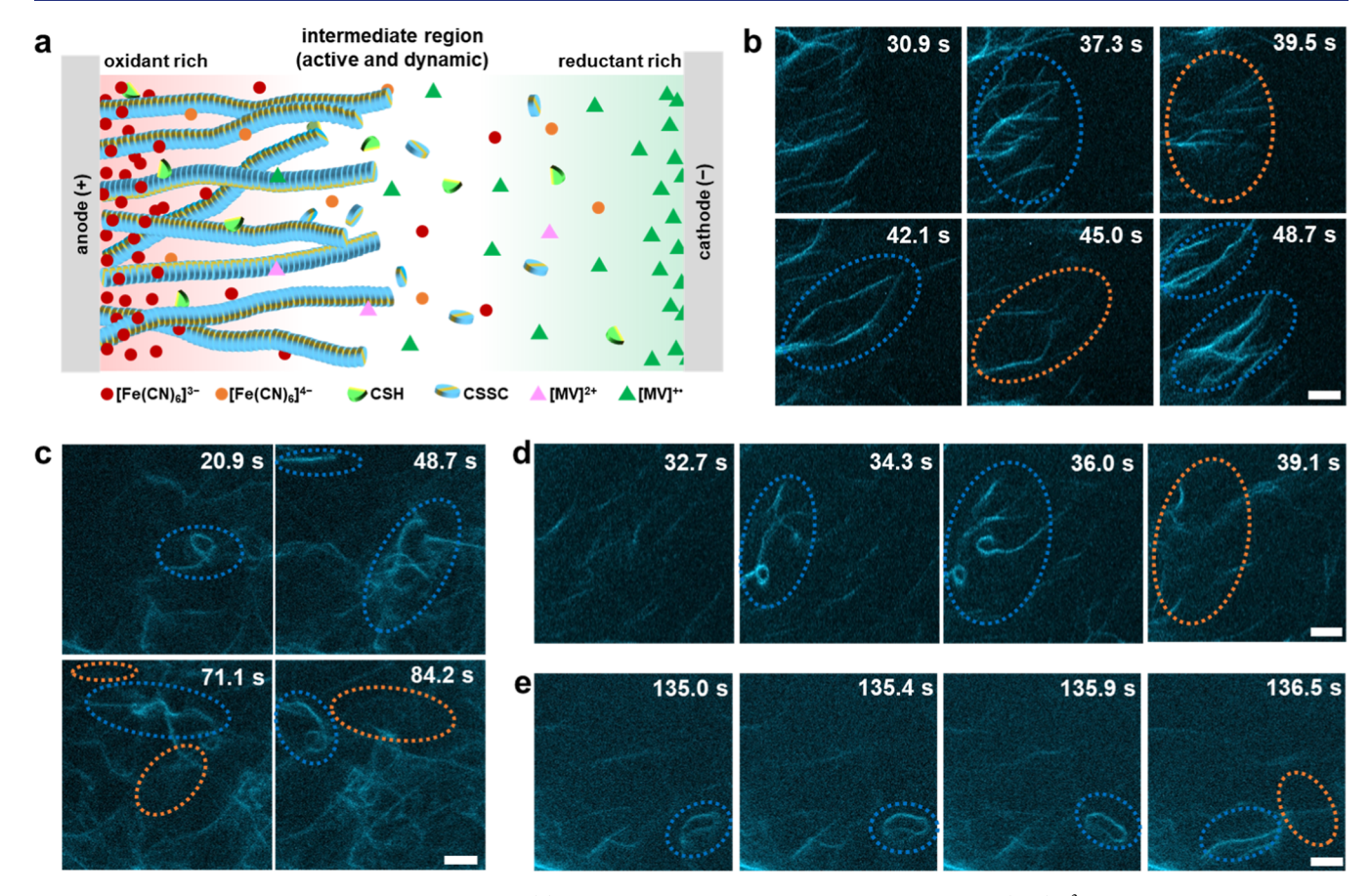


Figure 4. Fully e-fueled active, dynamic self-assembly. (a) Schematic illustration showing generation of  $[Fe(CN)_6]^{3-}$  oxidant-rich region,  $[MV]^{+\bullet}$  reductant-rich region, and their intermediate region upon e-fueled activation inducing CSH  $\leftrightarrow$  CSSC interconversions to achieve active self-assembly. (b–e) CLSM snapshots of fully e-fueled DSA system displaying active and dynamic features undergoing rapid growth and shrinkage of CSSC fibers from 2 mM CSH and 120 mM  $[Fe(CN)_6]^{4-}$  in phosphate buffer at pH 7 having 200 mM (b,c), 300 mM (d), and 400 mM (e) of  $[MV]^{2+}$  at an interelectrode gap of 300  $\mu$ m. CLSM objective is mounted at fiber fronts located ~200  $\mu$ m away from the anode for b, d, and e and in the body of gel located ~175  $\mu$ m from the anode for c. Dotted circles in blue highlight new CSSC fiber assemblies, and those in orange show disassembly. The anode/working electrode is located on the left side for all snapshots. The scale bar is 10  $\mu$ m.

and the impedance changes in cyclic experiments confirm the robustness and reversibility of the fully e-fueled DSA system. This is in contrast to chemical-fueled DSA closed systems for which the systems continuously evolve as the chemical fuels are constantly consumed and wastes gradually build up. Even in our previously reported hybrid e-fueled DSA system, the change of system was reflected by the shifting baselines in both fluorescence plot and EIS curves in multiple cycle experiments (see Figures 2d and 4d in ref 34).<sup>34</sup> For the hybrid system,<sup>34</sup> even though the oxidant fuel ([Fe(CN)<sub>6</sub>]<sup>3-</sup>) is constantly regenerated by the electrocatalytic cycle, the chemical reductant (DTT) is irreversibly consumed with time, causing the change of the system. Overall, the experiments in this section clearly demonstrate that the fully e-fueled DSA is stable and reversible, showing transient and directional fiber growth with precise temporal control.

Several control experiments were conducted to confirm that the observed assembly/disassembly indeed arose from CSSC/CSH redox cycle. First, under otherwise identical conditions except without CSH, no fiber formation was observed under the same electrical potential (Movie S2). Second, when  $[Fe(CN)_6]^{4-}$  was missing in the system, no fiber formation was observed as there was no oxidative electrocatalytic cycle to catalyze the oxidation of CSH to generate CSSC (Movie S3). Third, when no  $[MV]^{2+}$  was added to the system, the formed

CSSC fibers did not disassemble because of the absence of reductive half cycle (Movie S4).

Active and Dynamic Behavior of Fully e-Fueled DSA. As discussed earlier (Figures 2 and 3), the synchronous electrochemical formation of  $[Fe(CN)_6]^{3-}$  and  $[MV]^{+\bullet}$  results in dynamic interconversion between CSH and CSSC in the fully e-fueled DSA system. Upon applying an electrical potential, concurrent activation of both electrocatalysts gives rise to three regions in the electrochemical cell: an oxidant-rich region near the anode, a reductant-rich region near the cathode, and the intermediate bulk region (Figure 4a). While anodically generated  $[Fe(CN)_6]^{3-}$  quickly catalyzes CSH oxidation into CSSC for fiber assembly propagating from the anode surface, the simultaneously formed [MV]++ at the cathode needs time to diffuse toward the anode side in order to reduce CSCC and trigger disassembly. As a result, in the beginning, the rate of fiber assembly at the anodic region is much faster than that of fiber disassembly, which is in good agreement with our earlier model kinetic study (Figure 2d,e). The NACA model reactions displayed a faster rate  $(k_1 \approx 268)$ M<sup>-1</sup> s<sup>-1</sup>, Figure S4) of disulfide formation than the disulfideto-thiol decay process ( $k_2 \approx 22 \text{ M}^{-1} \text{ s}^{-1}$ , Figure S4). To match the fiber growth and disassembly kinetics, we optimized several parameters, including the concentration of the reduction catalyst [MV]<sup>2+</sup> and the interelectrode gap, to balance the fiber

disassembly and assembly kinetics. Specifically, we gradually increased the concentration of  $[MV]^{2+}$  and decreased the interelectrode gap to boost the reduction for fiber disassembly to better match the fiber growth kinetics. Through increasing  $[MV]^{2+}$  concentration, more catalytic reductant ( $[MV]^{+\bullet}$ ) was created at the cathode. By shortening the interelectrode gap, we reduced the diffusion pathlength so that  $[MV]^{+\bullet}$  could reach the CSSC fibers more quickly to induce disassembly. Conversely, as the CSSC fibers grow further away from the anode surface, it increases the pathlength for the catalytic oxidant ( $[Fe(CN)_6]^{3-}$ ) to reach the fiber fronts while the diffusion of  $[Fe(CN)_6]^{3-}$  through the gel is also slowed down, both factors leading to slower assembly as the fibers grow further. At some point, the fiber growth kinetics was just matched by the disassembly kinetics at the fiber fronts, and homeostasis was established (Figure 4a).

After full optimizations, under the following conditions (2 mM CSH, 120 mM  $[Fe(CN)_6]^{4-}$ , 200 mM  $[MV]^{2+}$ , and an interelectrode gap of 300  $\mu$ m), we achieved an active DSA showing high dynamic instability (Figure 4c, Movie S5). After applying 0.8 V (vs ITO reference) bias to the above system, CSSC fibers initially grew rapidly by positive fueling until the active growth was counter-balanced by reduction caused by [MV]<sup>+•</sup> (negative fuel) diffused from the cathode, reaching a dynamic steady state in the intermediate region (Figure 4a). High dynamic instability for the fiber assembly was observed not only at the fiber fronts (CLSM objective located  $\sim$ 200  $\mu$ m away from the anode and  $\sim$ 100  $\mu$ m from the cathode, Figure 4b,d,e and Movies S5, S7, and S8) but also toward the body of gel (CLSM objective located  $\sim 175 \mu m$  away from the anode and  $\sim$ 125  $\mu$ m from the cathode, Figure 4c and Movie S6). As shown by the videos, fibers stochastically shrunk and grew at the same time due to the fully e-fueled active process. Upon increasing the concentration of [MV]<sup>2+</sup> to 300 mM (Figure 4d, Movie S7) and 400 mM (Figure 4e, Movie S8), respectively, faster fiber disassembly was achieved and more complex dynamic features were observed, including concurrent growth and shrinkage, looping, and waving, due to an increased production of [MV]+• by e-fueling. Several physical factors such as concentration gradients of electrocatalysts created upon e-fueling, liquid-liquid phase separation caused by CSH sol to CSSC gel conversion and vice versa, 50 electrostrictive hydrodynamics,<sup>51</sup> and electroosmosis<sup>52</sup>—could also contribute to the complex out-of-equilibrium nature along with varied [MV]+• content. For control, an otherwise identical system except without [MV]2+ generated only static fibers with no dynamic feature (Movie S4), confirming the critical role of in situ generated [MV]+• in order to achieve dynamic active selfassembly.

Sustained Homeostasis for Waste-free, Fully e-Fueled DSA. Since the fully e-fueled DSA system is a waste-free closed-loop system that catalytically generates both the positive ([Fe(CN)<sub>6</sub>]<sup>3-</sup>) and negative fuels ([MV]<sup>+•</sup>) to power the DSA process, it offers a unique opportunity to create a sustained homeostatic active system lasting for an extended period of time. To demonstrate this, we used CLSM to monitor the active behavior of our DSA system under a constant bias of 0.8 V (vs ITO reference) for >4 h (Figure 5a, Movie S9). Specifically, at every 30 min interval, a 2 min CLSM video was taken for the active DSA system at the same focus area. The CLSM results confirm that the active and dynamic assemblies were sustained during the entire period (Figure 5a). The corresponding average fluorescence intensity

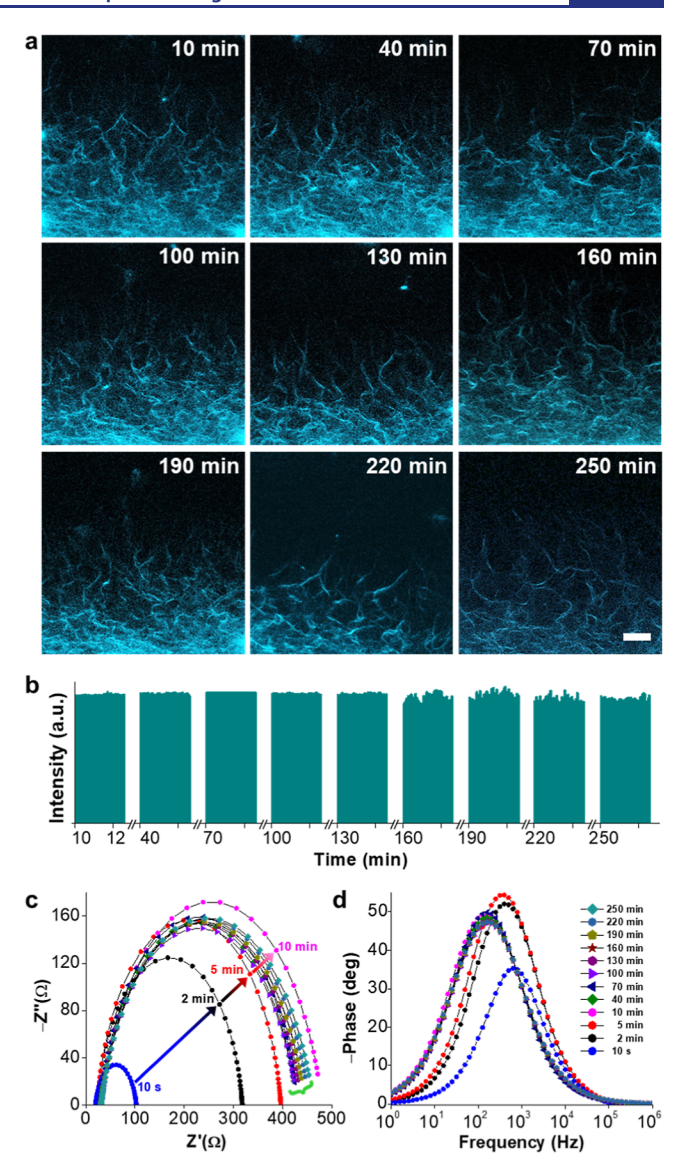


Figure 5. Sustained homeostasis for fully e-fueled DSA system. (a) Dynamic sustainability of CSSC fiber assembly growing and shrinking at once under constant 0.8 V vs ITO reference (phosphate buffer at pH 7, 2 mM CSH, 120 mM  $[Fe(CN)_6]^{4-}$ , 300 mM  $[MV]^{2+}$ , with an interelectrode gap of 300  $\mu$ m). Snapshots from CLSM analysis provided at ~30 min intervals show sustained dynamic behavior with continuous e-fueling. The anode and cathode are located at the bottom and top of CLSM objective, respectively. The scale bar is 10  $\mu$ m. (b) Corresponding average fluorescence intensity profiles derived from CLSM image frames extracted for the first 2 min after every ~30 min intervals, indicating retention of fluorescence arising from simultaneous growth and dissolution of CSSC fibers at steady state equilibrium up to 250 min of e-fueling. (c) Nyquist and (d) Bode plots derived for the same set of measurements at a frequency range of  $10^{0}$  to  $10^{6}$  Hz, with an AC perturbation of  $\pm 10$  mV. The arrows and green bracket respectively show an impedance increase up to 10 min and then retention up to 250 min of applying voltage.

values for each CLSM image frame for the monitored area (135  $\mu$ m × 135  $\mu$ m) recorded for 781.9 ms duration were compared at different time points (Figure 5b), showing nearly constant fluorescence intensity throughout the process. This confirms that the fully e-fueled system can sustain the homeostatic active state for an extended period of time because the positive (oxidation for fiber assembly) and

negative (reduction for disassembly) activities occur simultaneously with matching kinetics.

Finally, the sustained homeostasis for the active assembly was confirmed by EIS measurements that were conducted under a constant bias of 0.8 V (vs ITO reference) in the frequency range of  $10^{0}-10^{6}$  Hz at  $\sim 30$  min intervals to monitor impedance change caused by the growth of CSSC fibers. As shown in the Nyquist plots (Figure 5c), after an initial increase in the impedance in the first 10 min upon applying the voltage, it stabilized into relatively constant values for the next 4 h. The corresponding Bode plots (Figure 5d) showed a similar trend, with mid-frequency phase angle peaks increasing for the first 10 min and then remaining nearly constant for the remaining period. The EIS data are in good agreement with the CLSM data (Figure 5b). Right after applying a voltage to the DSA system, electrochemical oxidation-fueled fiber growth dominates, which increases charge-transfer resistance in the cell due to the non-conducting nature of CSSC fibers, resulting in enhanced impedance for ~10 min (Figure 5c,d). After that short period of time, sufficient negative fuel [MV]+• generating from the cathode diffused to the bulk solution to counter the fiber growth (the system eventually reaches the steady state), reaching a homeostatic active state showing constant impedance values (Figure 5c,d).

#### CONCLUSIONS

In summary, we developed a fully e-fueled DSA system employing two electrocatalytic cycles by simultaneously generating the positive fuel (oxidant) from the anode and the negative fuel (reductant) from the cathode. By coupling the synchronous electrocatalytic formation of oxidant [Fe- $(CN)_6$ <sup>3-</sup> and reductant  $[MV]^{+\bullet}$  with redox-controlled interconversion between CSH and CSSC, we achieved a fully e-fueled DSA system. The kinetic model study confirmed that the e-fueled interconversion between CSH and CSSC is robust and fully reversible for multiple cycles. Transient fiber assembly was shown by repetitively turning on and off the electrical voltage. Through balancing CSH oxidation by positive fuel for fiber assembly and CSSC reduction by negative fuel for fiber disassembly, dynamic active selfassembly was sustained by electrical potential. Compared to chemical-fueled synthetic DSA systems, the fully e-fueled DSA demonstrated here has several advantageous features. First, due to the complete electrocatalytic reaction cycles, no chemical waste is produced in the entire process. Second, the absence of waste generation allows us to achieve a homeostatic active DSA system that can be sustained for an extended period of time (>4 h), which was not possible for any previous synthetic closed-system active materials. Such a fully e-fueled, waste-free, and sustainable active material platform will be employed to investigate other redox-active supramolecular self-assembly systems which may open door to potential bioelectronic applications in the future. 53,54

#### ASSOCIATED CONTENT

#### Supporting Information

The Supporting Information is available free of charge at https://pubs.acs.org/doi/10.1021/jacs.2c13140.

Materials, design and fabrication of electrochemical cells, experimental methods, kinetic data, CLSM, EIS analysis, cryo-TEM (PDF)

(ZIP)

Transient formation of CSSC fiber assembly and disassembly under voltage on and off conditions using the fully e-fueled approach (MPG)

No fiber assembly under 0.8 V electric potential in the absence of CSH (MPG)

No fiber assembly under 0.8 V electric potential in the absence of  $[Fe(CN)_6]^{4-}$  (MPG)

No disassembly of CSSC fibers grown under 0.8 V electric potential in the absence of [MV]<sup>2+</sup> even after voltage turned off (MPG)

Generation of active and dynamic behavior at the fiber fronts under 0.8 V bias for the full system containing CSH,  $[Fe(CN)_6]^{4-}$ , and  $[MV]^{2+}$  (MPG)

Generation of active and dynamic behavior in the bulk of the fiber under 0.8 V bias for the full system containing CSH,  ${\rm [Fe(CN)_6]^{4-}}$ , and  ${\rm [MV]^{2+}}$  (MPG)

Active and dynamic behavior at the fiber fronts under 0.8 V bias for the full system containing CSH,  $[Fe(CN)_6]^{4-}$ , and slight excess of  $[MV]^{2+}$  (MPG)

Active and dynamic behavior under 0.8 V bias for the full system containing CSH,  $[Fe(CN)_6]^{4-}$ , and excess of  $[MV]^{2+}$  (MPG)

Sustainable active assembly for the full system containing CSH, [Fe(CN)<sub>6</sub>]<sup>4-</sup>, and [MV]<sup>2+</sup> under a constant electric potential of 0.8 V over 4 h (MPG)

#### AUTHOR INFORMATION

#### **Corresponding Author**

Zhibin Guan - Center for Complex and Active Materials, University of California Irvine, Irvine, California 92697, United States; Department of Chemistry, Department of Materials Science and Engineering, Department of Chemical and Biomolecular Engineering, and Department of Biomedical Engineering, University of California Irvine, Irvine, California 92697, United States; oorcid.org/0000-0003-1370-1511; Email: zguan@uci.edu

#### **Authors**

Dipankar Barpuzary - Center for Complex and Active Materials, University of California Irvine, Irvine, California 92697, United States; Department of Chemistry, University of California Irvine, Irvine, California 92697, United States; orcid.org/0000-0002-6276-7026

Paul J. Hurst - Department of Chemistry, University of California Irvine, Irvine, California 92697, United States; orcid.org/0000-0002-1826-2549

Joseph P. Patterson – Center for Complex and Active Materials, University of California Irvine, Irvine, California 92697, United States; Department of Chemistry and Department of Materials Science and Engineering, University of California Irvine, Irvine, California 92697, United States; orcid.org/0000-0002-1975-1854

Complete contact information is available at: https://pubs.acs.org/10.1021/jacs.2c13140

#### **Funding**

This work was financially supported by the National Science Foundation Materials Research Science and Engineering Center program through the UC Irvine Center for Complex and Active Materials (DMR-2011967), the U.S. Department of Energy, Office of Science, Basic Energy Sciences (DE-FG0204ER46162; Z.G.; feasibility study), and the National Science Foundation (CHE-1904939; Z.G.; kinetic study).

#### Notes

The authors declare no competing financial interest.

#### ACKNOWLEDGMENTS

The authors acknowledge the use of facilities and instrumentation at the UC Irvine Materials Research Institute (IMRI) supported in part by the National Science Foundation Materials Research Science and Engineering Center program through the UC Irvine Center for Complex and Active Materials (DMR-2011967). CLSM imaging analysis was made possible in part through access to the Optical Biology Core Facility of the Developmental Biology Center, a shared resource supported by the Cancer Center Support Grant (CA-62203) and the Center for Complex Biological Systems Support Grant (GM-076516) at the University of California, Irvine. D.B. and Z.G. thank Shane Ardo for helpful discussion and providing electrochemical cells with a potentiostat to conduct initial optimization experiments.

#### REFERENCES

- (1) Merindol, R.; Walther, A. Materials Learning from Life: Concepts for Active, Adaptive and Autonomous Molecular Systems. *Chem. Soc. Rev.* **2017**, *46*, 5588–5619.
- (2) van Esch, J. H.; Klajn, R.; Otto, S. Chemical Systems Out of Equilibrium. *Chem. Soc. Rev.* **2017**, *46*, 5474–5475.
- (3) Fletcher, D. A.; Geissler, P. L. Active Biological Materials. *Annu. Rev. Phys. Chem.* **2009**, *60*, 469–486.
- (4) Hess, H.; Ross, J. L. Non-Equilibrium Assembly of Microtubules: From Molecules to Autonomous Chemical Robots. *Chem. Soc. Rev.* **2017**. *46*, 5570–5587.
- (5) Boekhoven, J.; Hendriksen, W. E.; Koper, G. J. M.; Eelkema, R.; van Esch, J. H. Transient Assembly of Active Materials Fueled by A Chemical Reaction. *Science* **2015**, *349*, 1075–1079.
- (6) Rieß, B.; Grötsch, R. K.; Boekhoven, J. The Design of Dissipative Molecular Assemblies Driven by Chemical Reaction Cycles. *Chem* **2020**, *6*, 552–578.
- (7) Das, K.; Gabrielli, L.; Prins, L. J. Chemically Fueled Self-Assembly in Biology and Chemistry. *Angew. Chem., Int. Ed.* **2021**, *60*, 20120–20143.
- (8) Mattia, E.; Otto, S. Supramolecular Systems Chemistry. *Nat. Nanotechnol.* **2015**, *10*, 111–119.
- (9) Sharko, A.; Livitz, D.; De Piccoli, S.; Bishop, K. J. M.; Hermans, T. M. Insights into Chemically Fueled Supramolecular Polymers. *Chem. Rev.* **2022**, *122*, 11759–11777.
- (10) Klajn, R.; Wesson, P. J.; Bishop, K. J. M.; Grzybowski, B. A. Writing Self-Erasing Images using Metastable Nanoparticle "Inks". *Angew. Chem., Int. Ed.* **2009**, *48*, 7035–7039.
- (11) Ross, T. D.; Lee, H. J.; Qu, Z.; Banks, R. A.; Phillips, R.; Thomson, M. Controlling Organization and Forces in Active Matter Through Optically Defined Boundaries. *Nature* **2019**, *572*, 224–229.
- (12) Weißenfels, M.; Gemen, J.; Klajn, R. Dissipative Self-Assembly: Fueling with Chemicals versus Light. *Chem* **2021**, *7*, 23–37.
- (13) Ogden, W. A.; Guan, Z. Redox Chemical-Fueled Dissipative Self-Assembly of Active Materials. *ChemSystemsChem* **2020**, 2, No. e1900030.
- (14) Tena-Solsona, M.; Rieß, B.; Grötsch, R. K.; Löhrer, F. C.; Wanzke, C.; Käsdorf, B.; Bausch, A. R.; Müller-Buschbaum, P.; Lieleg, O.; Boekhoven, J. Non-Equilibrium Dissipative Supramolecular Materials with A Tunable Lifetime. *Nat. Commun.* **2017**, *8*, 15895.
- (15) Kariyawasam, L. S.; Hartley, C. S. Dissipative Assembly of Aqueous Carboxylic Acid Anhydrides Fueled by Carbodiimides. *J. Am. Chem. Soc.* **2017**, *139*, 11949–11955.

- (16) Bal, S.; Das, K.; Ahmed, S.; Das, D. Chemically Fueled Dissipative Self-Assembly that Exploits Cooperative Catalysis. *Angew. Chem., Int. Ed.* **2019**, *58*, 244–247.
- (17) Debnath, S.; Roy, S.; Ulijn, R. V. Peptide Nanofibers with Dynamic Instability through Nonequilibrium Biocatalytic Assembly. *J. Am. Chem. Soc.* **2013**, 135, 16789–16792.
- (18) Kubota, R.; Makuta, M.; Suzuki, R.; Ichikawa, M.; Tanaka, M.; Hamachi, I. Force Generation by A Propagating Wave of Supramolecular Nanofibers. *Nat. Commun.* **2020**, *11*, 3541.
- (19) Heinen, L.; Walther, A. Programmable Dynamic Steady States in ATP-Driven Nonequilibrium DNA Systems. *Sci. Adv.* **2019**, *5*, No. eaaw0590.
- (20) Del Grosso, E.; Prins, L. J.; Ricci, F. Transient DNA-Based Nanostructures Controlled by Redox Inputs. *Angew. Chem., Int. Ed.* **2020**, *59*, 13238–13245.
- (21) Grötsch, R. K.; Wanzke, C.; Speckbacher, M.; Angi, A.; Rieger, B.; Boekhoven, J. Pathway Dependence in the Fuel-Driven Dissipative Self-Assembly of Nanoparticles. *J. Am. Chem. Soc.* **2019**, *141*, 9872–9878
- (22) Sorrenti, A.; Leira-Iglesias, J.; Sato, A.; Hermans, M. Non-Equilibrium Steady States in Supramolecular Polymerization. *Nat. Commun.* **2017**, *8*, 15899.
- (23) Maiti, S.; Fortunati, I.; Ferrante, C.; Scrimin, P.; Prins, L. J. Dissipative Self-Assembly of Vesicular Nanoreactors. *Nat. Chem.* **2016**, *8*, 725–731.
- (24) Mishra, A.; Korlepara, D. B.; Kumar, M.; Jain, A.; Jonnalagadda, N.; Bejagam, K. K.; Balasubramanian, S.; George, S. J. Biomimetic Temporal Self-Assembly via Fuel-Driven Controlled Supramolecular Polymerization. *Nat. Commun.* **2018**, *9*, 1295.
- (25) te Brinke, E.; Groen, J.; Herrmann, A.; Heus, H. A.; Rivas, G.; Spruijt, E.; Huck, W. T. S. Dissipative Adaptation in Driven Self-Assembly Leading to Self-Dividing Fibrils. *Nat. Nanotechnol.* **2018**, *13*, 849–855.
- (26) Leira-Iglesias, J.; Tassoni, A.; Adachi, T.; Stich, M.; Hermans, T. M. Oscillations, Travelling Fronts and Patterns in A Supramolecular System. *Nat. Nanotechnol.* **2018**, *13*, 1021–1027.
- (27) Colomer, I.; Morrow, M.; Fletcher, P. A Transient Self-Assembling Self-Replicator. *Nat. Commun.* **2018**, *9*, 2239.
- (28) Ikegami, T.; Kageyama, Y.; Obara, K.; Takeda, S. Dissipative and Autonomous Square-Wave Self-Oscillation of a Macroscopic Hybrid Self-Assembly under Continuous Light Irradiation. *Angew. Chem., Int. Ed.* **2016**, *55*, 8239–8243.
- (29) de Jong, J. J. D.; Hania, P. R.; Pugzlys, A.; Lucas, L. N.; de Loos, M.; Kellogg, R. M.; Feringa, B. L.; Duppen, K.; van Esch, J. H. Light-Driven Dynamic Pattern Formation. *Angew. Chem., Int. Ed.* **2005**, *44*, 2373–2376.
- (30) Klajn, R.; Bishop, K. J. M.; Grzybowski, B. A. Light-Controlled Self-Assembly of Reversible and Irreversible Nanoparticle Suprastructures. *Proc. Natl. Acad. Sci. U.S.A.* **2007**, *104*, 10305–10309.
- (31) De, S.; Klajn, R. Dissipative Self-Assembly Driven by the Consumption of Chemical Fuels. *Adv. Mater.* **2018**, *30*, 1706750.
- (32) Lee, H.; Tessarolo, J.; Langbehn, D.; Baksi, A.; Herges, R.; Clever, G. H. Light-Powered Dissipative Assembly of Diazocine Coordination Cages. *J. Am. Chem. Soc.* **2022**, *144*, 3099–3105.
- (33) Kundu, P. K.; Das, S.; Ahrens, J.; Klajn, R. Controlling the Lifetimes of Dynamic Nanoparticle Aggregates by Spiropyran Functionalization. *Nanoscale* **2016**, *8*, 19280–19286.
- (34) Selmani, S.; Schwartz, E.; Mulvey, J. T.; Wei, H.; Grosvirt-Dramen, A.; Gibson, W.; Hochbaum, A. I.; Patterson, J. P.; Ragan, R.; Guan, Z. Electrically Fueled Active Supramolecular Materials. *J. Am. Chem. Soc.* **2022**, *144*, 7844–7851.
- (35) Chen, S.; Itoh, Y.; Masuda, T.; Shimizu, S.; Zhao, J.; Ma, J.; Nakamura, S.; Okuro, K.; Noguchi, H.; Uosaki, K.; Aida, T. Subnanoscale Hydrophobic Modulation of Salt Bridges in Aqueous Media. *Science* **2015**, *348*, 555–559.
- (36) Krabbenborg, S. O.; Veerbeek, J.; Huskens, J. Spatially Controlled Out-of-Equilibrium Host-Guest System under Electrochemical Control. *Chem.—Eur. J.* **2015**, *21*, 9638–9644.

- (37) Ragazzon, G.; Malferrari, M.; Arduini, A.; Secchi, A.; Rapino, S.; Silvi, S.; Credi, A. Autonomous Non-Equilibrium Self-Assembly and Molecular Movements Powered by Electrical Energy. *Angew. Chem., Int. Ed.* **2023**, *62*, No. e202214265.
- (38) Gortner, R. A.; Hoffman, W. F. An Interesting Colloid Gel. J. Am. Chem. Soc. 1921, 43, 2199–2202.
- (39) Llobell, A.; Fernandez, V. M.; López-Barea, J. Electron Transfer Between Reduced Methyl Viologen and Oxidized Glutathione: A New Assay of Saccharomyces Cerevisiae Glutathione Reductase. *Arch. Biochem. Biophys.* **1986**, 250, 373–381.
- (40) Benniston, A. C.; Hagon, J.; He, X.; Yang, S.; Harrington, R. W. Spring Open Two-Plus-Two Electron Storage in A Disulfide-Strapped Methyl Viologen Derivative. *Org. Lett.* **2012**, *14*, 506–509.
- (41) Hall, G. B.; Kottani, R.; Felton, G. A.; Yamamoto, T.; Evans, D. H.; Glass, R. S.; Lichtenberger, D. L. Intramolecular Electron Transfer in Bipyridinium Disulfides. *J. Am. Chem. Soc.* **2014**, *136*, 4012–4018.
- (42) Madasamy, K.; Velayutham, D.; Suryanarayanan, V.; Kathiresan, M.; Ho, K.-C. Viologen-Based Electrochromic Materials and Devices. *J. Mater. Chem. C* **2019**, *7*, 4622–4637.
- (43) Murakami, E.; Deppenmeier, U.; Ragsdale, S. W. Characterization of the Intramolecular Electron Transfer Pathway from 2-Hydroxyphenazine to the Heterodisulfide Reductase from Methanosarcina thermophila. *J. Biol. Chem.* **2001**, 276, 2432–2439.
- (44) Bird, C. L.; Kuhn, A. T. Electrochemistry of the Viologens. Chem. Soc. Rev. 1981, 10, 49-82.
- (45) Striepe, L.; Baumgartner, T. Viologens and Their Application as Functional Materials. *Eur. J. Chem.* **2017**, *23*, 16924–16940.
- (46) Mizuguchi, J.; Karfunkel, H. Semi-Empirical Calculations on the Optical Absorption of Methylviologen and *p*-Cyanophenylviologen in Different Oxidation States. *Bunsen-Ges. Phys. Chem., Ber.* **1993**, *97*, 1466–1472.
- (47) Luo, J.; Hu, B.; Debruler, C.; Bi, Y.; Zhao, Y.; Yuan, B.; Hu, M.; Wu, W.; Liu, T. L. Unprecedented Capacity and Stability of Ammonium Ferrocyanide Catholyte in pH Neutral Aqueous Redox Flow Batteries. *Joule* **2019**, *3*, 149–163.
- (48) Moon, H. C.; Lodge, T. P.; Frisbie, C. D. Solution Processable, Electrochromic Ion Gels for Sub-1 V, Flexible Displays on Plastic. *Chem. Mater.* **2015**, 27, 1420–1425.
- (49) Gélinas, B.; Das, D.; Rochefort, D. Air-Stable, Self-Bleaching Electrochromic Device Based on Viologen- and Ferrocene-Containing Triflimide Redox Ionic Liquids. *ACS Appl. Mater. Interfaces* **2017**, *9*, 28726–28736.
- (50) Saini, S.; Bukosky, S. C.; Ristenpart, W. D. Influence of Electrolyte Concentration on the Aggregation of Colloidal Particles Near Electrodes in Oscillatory Fields. *Langmuir* **2016**, *32*, 4210–4216.
- (51) Ristenpart, W. D.; Jiang, P.; Slowik, M. A.; Punckt, C.; Saville, D. A.; Aksay, I. A. Electrohydrodynamic Flow and Colloidal Patterning Near Inhomogeneities on Electrodes. *Langmuir* **2008**, *24*, 12172–12180.
- (52) Davidson, S. M.; Andersen, M. B.; Mani, A. Chaotic Induced-Charge Electro-Osmosis. *Phys. Rev. Lett.* **2014**, *112*, 128302.
- (53) Grzybowski, B. A.; Huck, W. T. The Nanotechnology of Life-inspired Systems. *Nat. Nanotechnol.* **2016**, *11*, 585–592.
- (54) Song, E.; Li, J.; Won, S. M.; Bai, W.; Rogers, J. A. Materials for Flexible Bioelectronic Systems as Chronic Neural Interfaces. *Nat. Mater.* **2020**, *19*, 590–603.

### **□** Recommended by ACS

## Nonlinear Transient Permeability in pH-Responsive Bicontinuous Nanospheres

Wouter P. van den Akker, Jan C. M. van Hest, et al.

MARCH 30, 2023

JOURNAL OF THE AMERICAN CHEMICAL SOCIETY

READ 🗹

#### **Chemically Fueled Reinforcement of Polymer Hydrogels**

Chamoni W. H. Rajawasam, Dominik Konkolewicz, et al.

FEBRUARY 27, 2023

JOURNAL OF THE AMERICAN CHEMICAL SOCIETY

READ 🗹

#### Switchable Hydrophobic Pockets in DNA Protocells Enhance Chemical Conversion

Wei Liu, Andreas Walther, et al.

MARCH 27, 2023

JOURNAL OF THE AMERICAN CHEMICAL SOCIETY

READ 🗹

## The Formation and Displacement of Ordered DNA Triplexes in Self-Assembled Three-Dimensional DNA Crystals

Yue Zhao, Ruojie Sha, et al

FEBRUARY 02, 2023

JOURNAL OF THE AMERICAN CHEMICAL SOCIETY

READ 🗹

Get More Suggestions >